Progress In Electromagnetics Research C, Vol. 63, 13–21, 2016

Practical Design of Filters Using EBG Waveguides Periodically Loaded with Metal Ridges

Stephan Marini[1, *], Pablo Soto[2], Ángela Coves[3], Benito Gimeno[4], and Vicente E. Boria[2]

Abstract—The dispersion diagram of infinite periodic structures is useful for the practical design of waveguide filters. Starting from the dispersion diagram of a unit cell, it is possible to generate a finite structure with very similar pass- and stop-bands (gaps). However, truncation of the infinite periodic structure degrades the pass-band performance. In this paper, these impairments are overcome by means of suitable waveguide tapers matching the impedance of the periodic structure to the access ports. As a result, the design of practical low-pass filters, derived from passive structures based on Electromagnetic Band-Gap (EBG) waveguides periodically loaded with metal ridges, is successfully addressed. According to this procedure, a five-order and an eight-order EBG low-pass filters are obtained after an optimization step. Measurements of a manufactured prototype fully validate the proposed approach.

1. INTRODUCTION

Periodic structures exhibit very attractive properties, such as compact size and enhanced out-of-band rejection, which have boosted interest in their potential use for filtering applications in microwave and millimetre-wave frequency bands. The excellent properties of such structures are related to the propagation of slow waves, which are characterized by a reduced phase velocity and wavelength. Using periodic structures, and due to the dispersive behaviour of their slow waves, it is possible to achieve filters with improved stop-band performance and reduced size [1–5]. Although the reported applications of slow-wave structures have been mainly focused on planar technologies, recently, it has been shown how to obtain Electromagnetic Band-Gap (EBG) passive waveguide structures by including metal inserts in the E-plane of an above cut-off rectangular waveguide [6–8]. These EBG ridged waveguide structures have a pass-band performance starting from the cut-off frequency of the housing waveguide, whereas the upper cutoff is defined from the unit cell dimensions together with the gap between the ridges. Even though the resulting response is pass-band in frequency terms, in microwave terminology it is commonly referred as a low-pass characteristic since it starts from the first frequency where the waveguide ports effectively propagate [9].

Ridged rectangular waveguide structures have been largely employed for practical filters due to their low fundamental-mode cutoff frequency, wide monomode bandwidth and compact size. As a result, there are well-established techniques for the design of several types of bandpass filters with metal inserts, such as evanescent-mode filters (i.e., with ridges inserted in a below-cutoff waveguide) [10–13] or E-plane filters including ridged resonators coupled by inductive strips [14, 15]. However, the design of practical low-pass filters with metal inserts in a hollow above-cutoff waveguide has not received the same attention in the technical literature. In fact, the periodic structures reported in [6–8] are unsuitable for

Received 16 November 2015, Accepted 16 March 2016, Scheduled 23 March 2016

* Corresponding author: Stephan Marini (smarini@ua.es).

[1] Departamento de Física, Ing. de Sistemas y Teoría de la Señal, IUFACyT, Universidad de Alicante, San Vicente del Raspeig, Alicante E-03690, Spain. [2] Departamento de Comunicaciones, iTEAM, Universidad Politécnica de Valencia, Camino de Vera, s/n, Valencia E-46022, Spain. [3] Departamento de Ingeniería de Comunicaciones, Universidad Miguel Hernández de Elche, Elche E-03202, Spain. [4] Departamento de Física Aplicada, ICMUV, Universidad de Valencia, Valencia E-46100, Spain.

practical applications in waveguide technology due to the severe degradation in the return loss level after truncation to a finite number of cells. Without imposing periodicity conditions, in [16] a conventional stepped impedance approach was proposed for the design of a maximally flat ridged low-order low-pass filter. Insertion loss techniques based on the distributed prototype, traditionally used for the design of classic corrugated waveguide low-pass filters [17, 18], could also be employed. However, they tend to provide conmensurated solutions (i.e., with equal electrical-length transmission lines) and have also limitations for very high order filters due to round-off errors in the analytical synthesis of the distributed prototype [17].

The purpose of this paper is to introduce a practical and simple technique for the design of low-pass filters with metal ridges in an above cut-off rectangular waveguide, which can be suitable for wide pass-bands and several numbers of cells (i.e., high order). The technique exploits the properties of EBG waveguides periodically loaded with metal inserts by using the pass-and stop-bands of the corresponding dispersion diagram. Once a suitable dispersion diagram for the infinite periodic structure is derived, and in contrast to [6–8], the Bloch impedance is then matched to the impedance of the access ports to obtain a practical filter (i.e., composed of a finite number of cells with acceptable return loss levels). To attain such a goal, after truncation of the periodic structure, a stepped ridged waveguide transformer is designed and added to the finite periodic structure. As a result, a practical low-pass filter derived from an EBG structure is finally obtained.

In order to compute the dispersion diagram of the unit cell, a modal hybrid analysis method has also been developed. It makes use of a revisited version of the Integral Equation (IE) technique for characterizing planar waveguide junctions [19], in combination with the Boundary Integral-Resonant Mode Expansion (BI-RME) method [20] for obtaining the modal chart of the ridged waveguides.

2. THEORY

2.1. Analysis of EBG Ridged Waveguides

Figure 1 shows the two-dimensional layout of the finite EBG waveguide periodically loaded with metal ridges considered in this paper. The structure also includes input and output transformers to standard waveguide ports. The ridges of length L_r and width w, are placed symmetrically in both the upper and lower walls, providing a gap separation d_r.

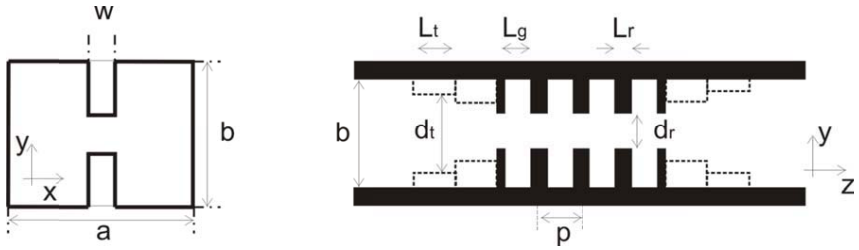

Figure 1. Two-dimensional layout and dimensions of a truncated Electromagnetic Band-Gap (EBG) waveguide periodically loaded with metal ridges. The finite EBG waveguide of period p is ended in stepped ridge tapers to match the impedance of the access ports.

The multimodal $ABCD$ chain matrix of one period p of the structure under study is directly obtained by solving the cascade connection of the waveguide sections and steps included in such a basic period (see Fig. 1):

$$\mathbf{M} = \begin{bmatrix} \mathbf{A} & \mathbf{B} \\ \mathbf{C} & \mathbf{D} \end{bmatrix} = \prod_{i=1}^{5} \begin{bmatrix} \mathbf{A}_i & \mathbf{B}_i \\ \mathbf{C}_i & \mathbf{D}_i \end{bmatrix} \tag{1}$$

where the elements of the first, third and fifth $ABCD$ matrices are trivial, since they correspond to hollow waveguides with finite lengths. On the other hand, the second and fourth matrices are related to the modelling of the same planar waveguide junction between the rectangular and the ridge waveguide.

In order to obtain the full-wave characterization of the involved planar junction, a very efficient method based on an integral equation technique is followed [19]. The application of this full-wave analysis method requires the knowledge of the modal charts of the waveguides involved in the planar junction under consideration, as well as the coupling coefficients between the modes of such waveguides. To obtain this information, the well-known Boundary Integral-Resonant Mode Expansion (BI-RME) technique has been employed [20]. Following all these methods, the generalized multimode Z-matrix of the planar waveguide junction is first determined, and next the full-wave two-port $ABCD$ parameters of such junction are numerically derived as follows:

$$\begin{aligned} \mathbf{A} &= \mathbf{Z}_{11} \cdot \mathbf{Z}_{21}^{-1} \\ \mathbf{B} &= \mathbf{Z}_{11} \cdot \mathbf{Z}_{21}^{-1} \cdot \mathbf{Z}_{22} - \mathbf{Z}_{12} \\ \mathbf{C} &= \mathbf{Z}_{21}^{-1} \\ \mathbf{D} &= \mathbf{Z}_{21}^{-1} \cdot \mathbf{Z}_{22} \end{aligned} \tag{2}$$

In a periodic structure of period p, we can impose the Floquet condition [21], then:

$$\begin{pmatrix} \mathbf{V}_1 \\ \mathbf{I}_1 \end{pmatrix} = \mathbf{M} \begin{pmatrix} \mathbf{V}_2 \\ -\mathbf{I}_2 \end{pmatrix} = e^{\gamma p} \begin{pmatrix} \mathbf{V}_2 \\ -\mathbf{I}_2 \end{pmatrix} \tag{3}$$

where γ is the propagation constant of the Floquet modes of the infinite periodic structure.

The right-hand side of Eq. (3) can be expressed in the classical canonical form

$$\mathbf{M} \cdot \mathbf{x} = \mathbf{\Lambda} \cdot \mathbf{I} \cdot \mathbf{x} \tag{4}$$

where $\mathbf{I}$ is the identity matrix. The solutions ($\mathbf{\Lambda}$ and $\mathbf{x}$) of the standard eigenvalue problem in Eq. (4), which are related to the required propagation constants and transverse field distributions in the periodic structure, respectively, can be determined straight forwardly by using well-established routines.

At a given frequency, the real and imaginary parts of the propagation constant, i.e., $\gamma = \alpha + j\beta$, corresponding to a Floquet mode are directly related to the vector component Λ_i as

$$\alpha_i = \frac{\ln|\Lambda_i|}{p} \quad \beta_i = \frac{\angle\Lambda_i}{p}. \tag{5}$$

The frequency ranges where at least a Floquet mode propagates provide different pass-bands of the periodic structure. Conversely, the stop-bands are characterized by the lack of propagating Floquet modes (i.e., non-trivial solutions of Eq. (4)). Therefore, in order to characterize the behaviour of the periodic structure in a given frequency range, the dispersion diagram resulting from the solution of the linear eigenvalue problem (4) must be computed on a frequency by frequency basis [22].

It must be pointed out that the technique just described takes into account rigorously both propagating and relevant evanescent modes at each frequency point. As a result, the computed parameters of the dispersion diagram also include the effect of the evanescent-modes in the pass-band and band-gap regions.

2.2. Finite Structure and Connection with Input/Output Rectangular Waveguide

The next step is the analysis of a real structure composed of a finite number of cells, which is connected to standard access ports. The number of cells after truncation is related with the attenuation to be attained in the band gap. However, the scattering parameters of the truncated structure are usually unsatisfactory for practical applications. In such a case, we propose adding an external input/output transformer while keeping the periodicity of the filtering structure, in order to gradually modify the impedance level from the waveguide port to the periodic part of the structure. To apply this procedure, we first compute the Bloch impedance of the first Floquet mode of the periodic structure using the eigenvectors V_{2i} and I_{2i} obtained from (3). This Bloch impedance must then be matched to the TE_{10} characteristic impedance (defined as the voltage to current ratio) of the input/output rectangular waveguide

$$Z_{\mathrm{TE}_{10}} = \frac{V}{I} = \frac{\pi b}{2a} \frac{\omega\mu_0}{\sqrt{\omega^2\mu_0\varepsilon_0 - \left(\frac{\pi}{a}\right)^2}}. \tag{6}$$

Such adaptation can be obtained, as a first approximation, from the design of an ideal quarter-wavelength stepped ridged waveguide transformer or a short-step ridged waveguide transformer [9, 23]. To obtain an initial guess of the transformer physical dimensions, one can find different works in the technical literature relating the dimensions of the ridges and the corresponding characteristic impedance. For this work we have used Hoefer formulation [24], in which the characteristic impedance (as voltage-to-current ratio) is computed as:

$$Z_0 = \frac{Z_{0\infty}}{\sqrt{\left(1-(\lambda/\lambda_{cr})^2\right)}} \tag{7}$$

being λ_{cr} the ridge wavelength at its cutoff frequency and $Z_{0\infty}$ the characteristic impedance at infinite frequency. This last parameter can be obtained by

$$Z_{0\infty} = 120\pi^2 \frac{K1}{K2} \tag{8}$$

where the constants $K1$ (the normalize cut-off ridge wavelength) and $K2$ have the closed-form expressions derived in [24] and [25]:

$$K1 = \frac{b}{\lambda_{cr}} = \frac{b}{2(a-w)}\left[1+\left(2.45+0.2\frac{w}{a}\right)\left(\frac{wb}{d_t(a-w)}\right)+\frac{4}{\pi}\left(1+0.2\sqrt{\frac{b}{a-w}}\right)\frac{b}{a-w}\ln\csc\left(\frac{\pi d_t}{2b}\right)\right]^{-\frac{1}{2}}$$

$$K2 = \frac{b}{d_t}\sin\left(\frac{\pi w}{b}\frac{b}{\lambda_{cr}}\right)+\left[\left(2\frac{b}{\lambda_{cr}}\right)\ln\csc\left(\frac{\pi d_t}{2b}\right)+\tan\left(\frac{\pi}{2}\frac{b}{\lambda_{cr}}\frac{a-w}{b}\right)\right]\cdot\cos\left(\frac{\pi w}{b}\frac{b}{\lambda_{cr}}\right)$$

and w and d_t are the ridge width and gap, respectively.

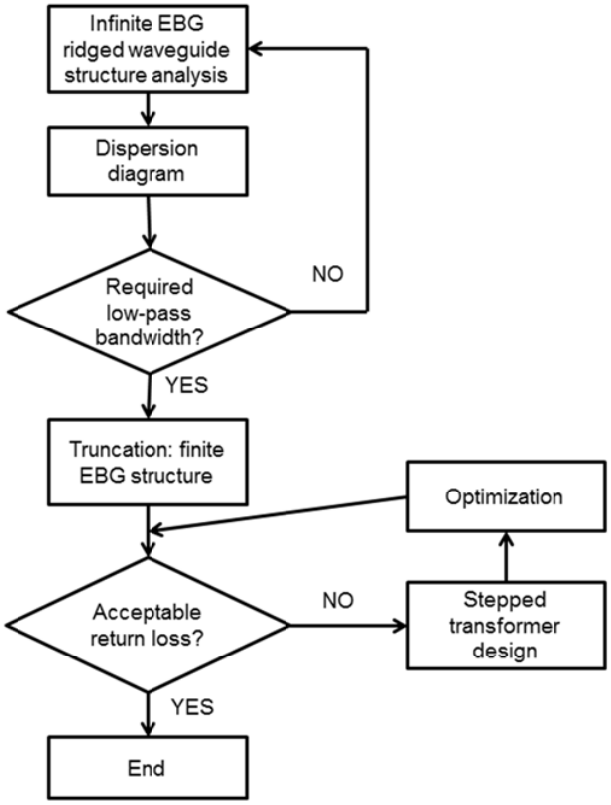

Figure 2. Flowchart of the whole design process employed.

The final result is obtained after an optimization process (simplex algorithm) of the parameters corresponding to the taper waveguide sections (their lengths L_t and gaps between ridge insertions d_t) using FEST3D [26]. This full-wave optimization considers rigorously the effect of the higher-order modes in the discontinuities (including also the attenuation factor of the evanescent ones), and the impedance variations along the taper sections.

As a summary, Fig. 2 shows a flowchart indicating the step-by-step design process.

3. RESULTS

In order to demonstrate the practical application of an EBG structure, a WR-90 rectangular waveguide periodically loaded with symmetrical ridges has been first considered. In this example the period of the unit cell is $p = 8\,\text{mm}$, all the insertions have the same width $w = 0.5\,\text{mm}$, length $L_r = 2\,\text{mm}$ and are separated $d_r = 1\,\text{mm}$. Fig. 3(a) shows the dispersion diagram of this EBG structure computed using the technique described in Section 2. These results are confirmed by the commercial software HFSS [27]. From Fig. 3(a) we can state that the EBG has a first pass-band from 5 to about 10.2 GHz, and presents a second pass-band from 14.5 GHz (due to the propagation of the second Floquet mode).

In the next step, we have transformed the infinite EBG into a real filter, i.e., considering only a finite number of cells (5 in this case, resulting in a fifth-order low-pass filter), and taking advantage of the existence of the first pass-band. The filter has a low-pass performance whose pass-band lower cutoff frequency coincides with the TE_{10} cut-off frequency of the WR-90 input/output rectangular waveguide, and the upper cut-off frequency is the same of the first EBG pass-band. The truncation of the infinite periodic structure highly degrades the reflection behaviour in the pass-band (see blue lines in Fig. 2(b)). In [6], to achieve a better impedance matching between the input/output WR-90 waveguides and the EBG, the authors proposed reducing by half the lengths of the first and last ridges with respect to the remaining ridges. This solution keeps the periodicity of the inner structure if the basic cell p defined in Fig. 1 is used (although the number of cells is then reduced to 4). However, as seen in the same Fig. 3(b) with black lines, in this case, the resulting filter still presents an unacceptable return loss level. After a quantitative analysis and an optimization process performed with FEST3D, we found that the best choice for both lengths L_{r1} and L_{r5} is 0.77 mm (red lines in Fig. 3(b)), improving the pass-band reflection in a short band (9.25–9.93 GHz). Nevertheless, this result clearly demonstrates that only by

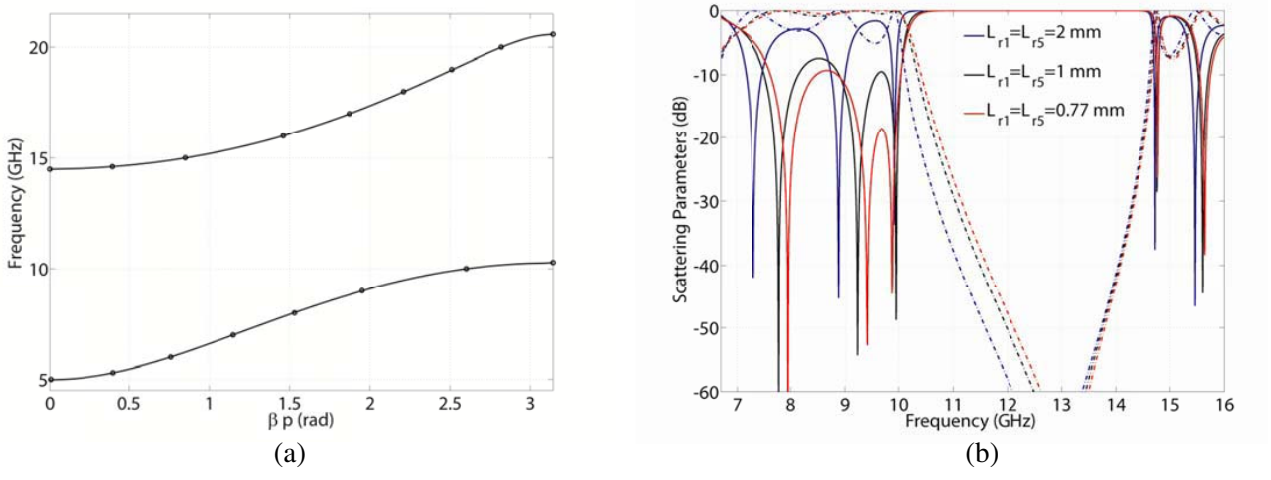

(a) (b)

Figure 3. (a) Dispersion behaviour (βp versus f) for a WR-90 waveguide periodically loaded with symmetrical ridges. With circles results from HFSS. (b) Electrical response ($|S_{21}|$ parameter in dashed lines) of the fifth-order EBG low-pass filter varying the length dimension of the first (L_{r1}) and last ridges (L_{r5}). With blue lines a structure with all identical ridges ($L_{r1} = L_{r5} = 2\,\text{mm}$); with black lines a similar solution to the one proposed in [6] ($L_{r1} = L_{r5} = 1\,\text{mm}$); with red lines the best option found by optimization ($L_{r1} = L_{r5} = 0.77\,\text{mm}$).

tuning the first and last ridge lengths it is impossible to reach acceptable return loss levels for filtering applications in a wide band.

In this paper, as a potential solution we propose to add a stepped transformer to the finite periodic structure with half-length input and output ridges (see Fig. 1). The transformer includes ridged waveguides with the same width w and different gaps d_t. With this solution, the periodicity p of the unit cell of the infinite structure is still maintained.

Figure 4 shows the final result after the optimization step (carried out with FEST3D tool) on a single stage quarter-wavelength transformer. The design specification was a level of $|S_{11}|$ below $-20\,\mathrm{dB}$ in the pass-band for the whole component. These results are also confirmed by the commercial software HFSS. Note that only one section has been required to obtain a good matching over such a wide bandwidth, being the length of the section $L_{t1} = 18.914\,\mathrm{mm}$ and its ridge gap $d_{t1} = 6.613\,\mathrm{mm}$.

A prototype of this low-pass filter has been manufactured in three pieces of brass using a milling machine. Fig. 5(a) shows the manufactured component, whereas Fig. 5(b) compares the simulated and

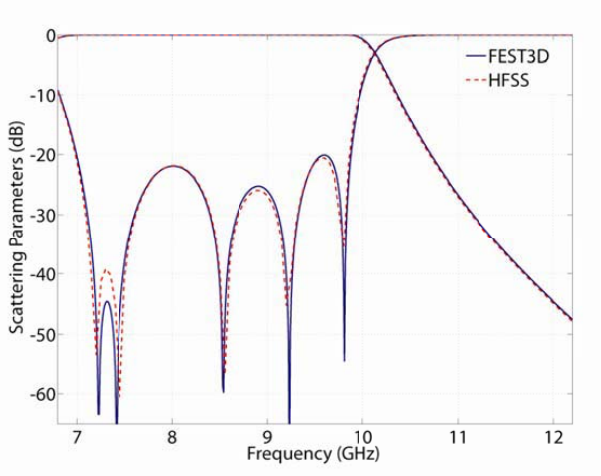

Figure 4. Electrical response of the fifth-order EBG low-pass filter after adding one-stepped ridged transformer.

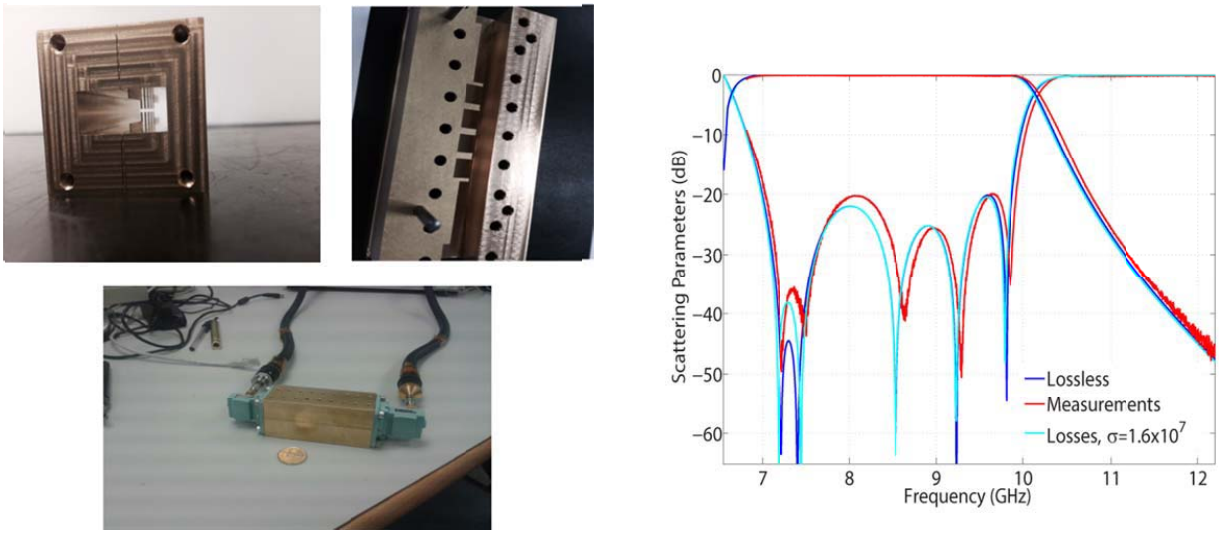

(a) (b)

Figure 5. (a) Pictures of the fifth-order EBG manufactured low-pass filter. (b) Simulations (lossless case and with a finite conductivity value of $\sigma = 1.6 \times 10^7\,\mathrm{S/m}$) and measurements of the filter electrical response.

measured response of this optimized low-pass filter (lossless case, and also assuming a finite conductivity value of $\sigma = 1.6 \times 10^7$ S/m (brass conductivity)). In this last case, the propagation losses have been computed using a technique based on the perturbation of boundary conditions [28, 29].

In Fig. 5(b), measurements have been obtained using a Vectorial Network Analyzer with a WR-90 TRL calibration kit. The agreement between simulated and measured performances is very good, and only an upwards shift of 50 MHz is observed in the measured response of the filter, which can be attributed to manufacturing tolerances. Insertion loss level is above 0.15 dB in the entire filter pass-band. These results fully validate the proposed approach.

Finally, we have designed a more demanding K-band filter by periodically loading a WR-34 ($a = 8.636$ mm and $b = 4.318$ mm) rectangular waveguide with symmetrical ridges. Fig. 6(a) shows the dispersion diagram of the infinite periodic structure whose cell has the following dimensions: $p = 5$ mm, $L_g = 3$ mm, $w = 0.2$ mm and $d_r = 1.2$ mm. In this second example, we can see that the first pass-band ranges from 14.5 to 25 GHz, and the second pass-band is present from 36.5 GHz. In Fig. 6(a) we have also displayed the dispersion diagram of the same structure considering high propagation losses (a finite conductivity of $\sigma = 10^6$ S/m has been simulated).

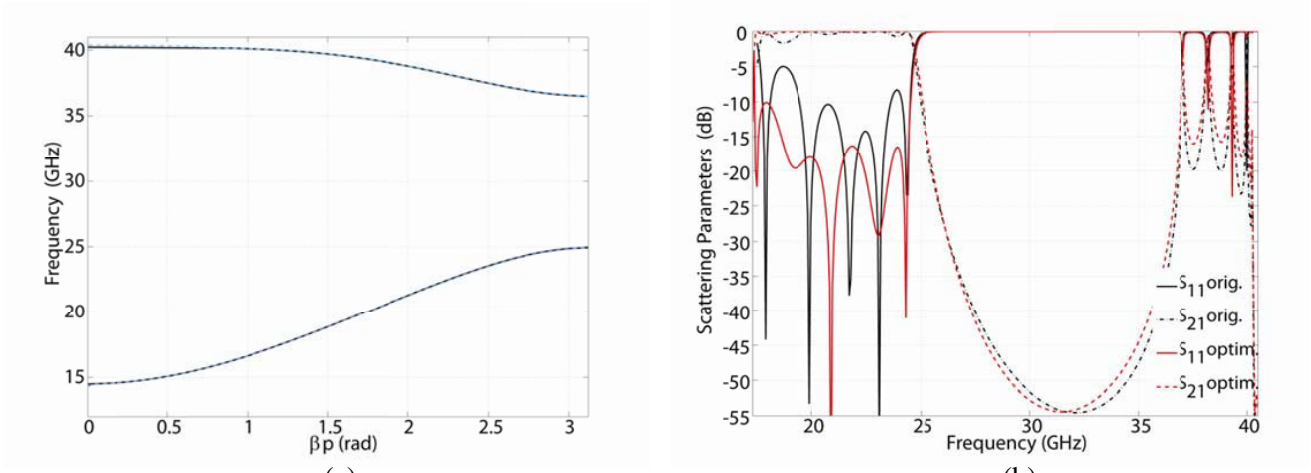

(a) (b)

Figure 6. (a) Dispersion behaviour (βp versus f) for a WR-34 waveguide periodically loaded with symmetrical ridges. In dashed blue lines we have also simulated the effect of propagation losses (finite conductivity of $\sigma = 10^6$ S/m). (b) Electrical response of the eight-order EBG low-pass filter before and after adding a two-section short-step ridged transformer optimized with FEST3D.

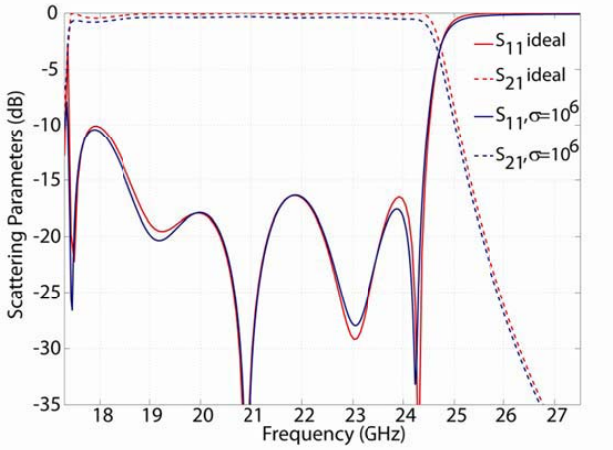

Figure 7. Magnitude of the scattering parameters of the eight-order EBG low-pass filter with a short-step ridged waveguide transformer considering the lossless case and propagation losses.

From the information provided by the dispersion diagram, we have designed an eight-order low-pass filter (8 unit cells) providing more selectivity than for the previous example. Fig. 6(b) shows the filter electrical response before and after adding a two-stage short-step ridged transformer optimized with FEST3D ($L_{t1} = 3.17\,\text{mm}$, $L_{t2} = 3.99\,\text{mm}$, $d_{t1} = 2.968\,\text{mm}$ and $d_{t2} = 3.728\,\text{mm}$, respectively). As it can be seen, the periodic filter loaded with optimized input and output tapers, has achieved a return loss level better than 17 dB in an extremely wide pass-band. Note also that the input and output tapers added to the periodic structure affect mainly to the passband return loss, while keeping the stopband performance essentially unaltered.

In Fig. 7 we compare the magnitude of the scattering parameters of this optimized low-pass filter considering the lossless case, as well as a real structure with a finite conductivity value of $\sigma = 10^6\,\text{S/m}$. A downwards frequency shift of about 52.5 MHz is observed in the simulated response with finite conductivity, whereas the insertion loss increases to 0.37 dB.

4. CONCLUSIONS

In this work, we have designed practical low-pass filters from the dispersion diagram of rectangular waveguides periodically loaded with metal ridges. The proposed design technique has been validated with two examples. In the first case, we have improved the pass-band performance of aperiodic structure by adding a step ridged waveguide transformer to its input and output stages. Using this approach, we have also designed a second higher order wideband filter for more demanding K-band applications, thus demonstrating the practical application of EBG ridged waveguide structures. The proposed procedure has been fully validated by means of measurements of a manufactured prototype.

ACKNOWLEDGMENT

This work was supported by the Ministerio de Economía y Competitividad (MINECO), Spanish Government, under the R&D projects TEC2013-47037-C5-1-R and TEC2013-47037-C5-4-R. The authors would like to thank ITACA (Instituto de Aplicaciones de las Tecnologías y de las Comunicaciones Avanzadas), from Technical University of Valencia (Valencia, Spain), for their support in the accurate manufacturing of the low-pass filter prototype.

REFERENCES

1. Wang, C.-C., H.-C. Chiu, and T.-G. Ma, "A slow-wave multilayer synthesized coplanar waveguide and its applications to rat-race coupler and dual-mode filter," *IEEE Trans. Microwave Theory Tech.*, Vol. 59, No. 7, 1719–1729, 2011.
2. Chang, W. S. and C.-Y. Chang, "Novel microstrip periodic structure and its application to microwave filter design," *IEEE Microw. Wireless Comp. Lett.*, Vol. 21, No. 3, 124–126, 2011.
3. Kurra, L., M. P. Abegaonkar, A. Basu, and S. K. Koul, "Switchable and tunable notch in ultra-wideband filter using electromagnetic bandgap structure," *IEEE Microw. Wireless Comp. Lett.*, Vol. 24, No. 12, 839–841, 2014.
4. Gao, M.-J., L.-S. Wu, and J. F. Mao, "Compact notched ultra-wideband bandpass filter with improved out-of-band performance using quasi electromagnetic bandgap structure," *Progress In Electromagnetics Research*, Vol. 125, 137–150, 2012.
5. Moghadasi, S. M., A. R. Attari, and M. M. Mirsalehi, "Compact and wideband 1-D mushroom-like EBG filters," *Progress In Electromagnetics Research*, Vol. 83, 323–333, 2008.
6. Goussetis, G., G. Feresidis, and P. Kosmas, "Efficient analysis, design, and filter applications of EBG waveguide with periodic resonantloads," *IEEE Trans. Microwave Theory Tech.*, Vol. 54, No. 11, 3885–3892, 2006.
7. Tang, Y. M., Y. M. Yu, and W. Wu, "Improved EBG-loaded waveguide low-pass filter," *Microwave and Optical Techn. Lett.*, Vol. 50, No. 8, 2090–2093, 2008.
8. Marini, S., A. Coves, M. Taroncher, V. E. Boria, and B. Gimeno, "Full-wave analysis and applications of EBG waveguides periodically loaded with metal ridges," *Proceeding of IEEE*

MTT-S Int. Microwave Workshop Series on Signal Integrity and High-Speed Interconnects, 87–90, Guadalajara, Mexico, 2009.

9. Matthaei, G. L., L. Young, and E. M. T. Jones, *Microwave Filters, Impedance-matching Networks, and Coupling Structures*, Artech House, Norwood, 1980.
10. Craven, G., *Evanescent Mode Microwave Components*, Artech House, Norwood, 1987.
11. Bornemann, J. and F. Arndt, "Transverse resonance, standing wave, and resonator formulations of the ridge waveguide eigenvalue problem and its application to the design of E-plane finned waveguide filters," *IEEE Trans. Microwave Theory Tech.*, Vol. 38, No. 8, 1104–1113, 1990.
12. Nanan, J.-C., J.-W. Tao, H. Baudrand, B. Theron, and S. Vigneron, "A two-step synthesis of broadband ridged waveguide bandpass filters with improved performances," *IEEE Trans. Microwave Theory Tech.*, Vol. 39, No. 12, 2192–2197, 1991.
13. Fahmi, M. M., J. A. Ruiz-Cruz, R. R. Mansour, and K. A. Zaki, "Compact ridge waveguide filters with arbitrarily placed transmission zeros using nonresonating nodes," *IEEE Trans. Microwave Theory Tech.*, Vol. 57, No. 12, 3354–3361, 2009.
14. Goussetis, G. and D. Budimir, "E-plane manifold multiplexers with improved bandwidth," *Proc. 31st Eur. Microwave Conf.*, 1–4, London, 2001.
15. Goussetis, G. and D. Budimir, "Novel periodically loaded E-plane filters," *IEEE Microwave and Wireless Comp. Lett.*, Vol. 13, No. 6, 193–195, 2003.
16. Yazdani, M., L. Murphy, A. Mallahzadeh, E. Arvas, and J. Mautz, "The design of double ridge waveguide filter using conventional stepped impedance low-pass filter method," *Microwave and Optical Techn. Lett.*, Vol. 56, No. 1, 120–124, 2014.
17. Cameron, R., C. Kudsia, and R. R. Mansour, *Microwave Filters: Fundamentals, Design and Applications*, John Wiley & Sons, Hoboken, 2007.
18. Monerris, O., P. Soto, S. Cogollos, V. E. Boria, J. Gil, C. Vicente, and B. Gimeno, "Accurate circuit synthesis of low-pass corrugated waveguide filters," *Proc. 40th Eur. Microwave Conf.*, 1237–1240, Paris, 2001.
19. Gerini, G., M. Guglielmi, and G. Lastoria, "Efficient integral equation formulations for admittance or impedance representation of planar waveguide junctions," *Proceeding of IEEE MTT-S Int. Microwave Symp. Digest, 1998*, Vol. 3, 1747–1750, Baltimore, MD, 1998.
20. Cogollos, S., S. Marini, V. E. Boria, P. Soto, A. Vidal, H. Esteban, et al., "Efficient modal analysis of arbitrarily shapedwaveguides composed of linear, circular and elliptical arcs using the BI-RME method," *IEEE Trans. Microwave Theory Tech.*, Vol. 51, No. 12, 2378–2390, 2003.
21. Collin, R. E., *Field Theory of Guided Waves*, McGraw-Hill, New York, 1960.
22. Marini, S., A. Coves, B. Gimeno, and V. E. Boria, "Efficient modal analysis of periodic structures loaded with arbitrarily shaped waveguides," *IEEE Trans. Microwave Theory Tech.*, Vol. 58, No. 3, 529–536, 2010.
23. Collin, R. E., *Foundations for Microwave Engineering*, McGraw-Hill, New York, 1992.
24. Hoefer, W. J. R. and M. N. Burton, "Closed-form expressions for the parameters of finned and ridged waveguides," *IEEE Trans. Microwave Theory Tech.*, Vol. 30, No. 12, 2190–2194, 1982.
25. Sharma, A. K. and W. J. R. Hoefer, "Empirical expressions for fin-line design," *IEEE Trans. Microwave Theory Tech.*, Vol. 31, No. 4, 350–356, 1983.
26. FEST3D 6.7. Aurora Software and Testing S.L. (on behalf of ESA/ESTEC), Valencia, Spain, [Online].
27. Ansys HFSS, (High Frequency Structure Simulator), Ansys Inc., Canonsburg, PA, USA.
28. Marini, S., M. Mattes, B. Gimeno, and V. E. Boria, "Improved computation of propagation losses in waveguide structures using perturbation of boundary conditions," *IEEE Microw. Wireless Comp. Lett.*, Vol. 21, No. 11, 577–579, 2011.
29. Marini, S., P. Soto, M. Mattes, B. Gimeno, S. Bleda, A. Vidal, and V. E. Boria, "Rigorous evaluation of propagation losses in arbitrarily shaped waveguide structures using boundary integral-resonant mode expansion and perturbation of boundary conditions," *IET Microwave, Antennas and Propagation*, Vol. 8, No. 12, 980–989, 2014.